PHYSICAL REVIEW A VOLUME 20, NUMBER 5 NOVEMBER 1979

Relativistic many-body investigation of the hyperfine interaction in ground-state rubidium

Mina Vajed-Samii, S. N. Ray,* and T. P. Das
Department of Physics, State University of New York, Albany, New York 12222

J. Andriessen
Laboratorium voor Technische Natuurkunde, Technische Hogeschool, Delft, The Netherlands
(Received 8 December 1978)

The hyperfine structure of the rubidium atom in the ground state has been studied by means of the relativistic many-body perturbation procedure. Relativistic effects are found to have an important influence on direct, exchange-core-polarization (ECP), and correlation effects, the enhancement over nonrelativistic results being, respectively, 20, 19, and 15%. Correlation effects are found to be significantly larger in magnitude as compared to ECP effects, the ratio of the two to the direct contribution being 0.32 and 0.19, respectively. This feature is opposite in nature to that in lithium and sodium, but represents a continuation of the trend found in going from lithium to sodium, and indicates that the relative importance of correlation will be even more pronounced in the heavier alkali metals, cesium and francium. The net theoretical value for the hyperfine constant was obtained as 3460 ± 50 MHz, in satisfactory agreement with the experimental result of 3417 MHz. The physical reasons for the observed trends in the contributions from different mechanisms will be discussed, including some detailed features such as the relative contributions from different core shells to the ECP and correlation effects.

I. INTRODUCTION

The study of alkali-metal atoms and alkali metals is pivotal to the understanding of the theory of hyperfine interactions[1] in atomic and solid-state systems in general. This is because in these relatively simple systems one can study the contributions of the different physical effects,[1-3] such as the direct, exchange-polarization, and many-body effects, in considerable detail without excessive effort. One hopes from such a study in these systems to obtain general conclusions regarding the relative importance of these physical effects, which can be useful in the study of more complicated systems. The present work is concerned with alkali-metal atoms, specifically rubidium, as part of our continuing efforts to understand the origin of hyperfine interactions in the alkali series, our earlier work[2] having been concerned with the lighter atoms lithium and sodium.

From earlier investigations,[4] it has been shown that the leading contribution to the hyperfine constant in alkali-metal atoms, and the simplest to calculate, is the direct contribution of the valence s electron. Using nonrelativistic Hartree-Fock (HF) theory, it has been found that this contribution ranges from 70% in lithium to 45% of the experimental result in cesium. The counterpart of the Casimir relativistic enhancement factor[5] in the framework of the HF theory is usually obtained by comparing the contact contributions from nonrelativistic and relativistic Hartree-Fock formalisms. Such an analysis shows[4-6] that the relativistic enhancement factors for the valence-electron contributions range from 0.1% in lithium to about 40% in the heaviest atom of this series, cesium.

The various effects that one has to consider beyond the direct mechanism arise from electron-electron interactions. The earlier investigations of these various effects have been carried out on[2] lithium and sodium using nonrelativistic many-body perturbation theory, the former having also been studied by other many-body procedures.[7] It has been found that a combination of direct, exchange-core-polarization (ECP), and correlation contributions produces good agreement with the experimental hyperfine constants. In these two atoms ECP effects are stronger than correlation effects, the relative importance of correlation appearing to be greater in sodium as compared to lithium.

In view of these results regarding the importance of ECP and correlation in the lighter alkali-metal atoms and the influence of relativistic effects on the direct contribution in the heavier ones, it is clear that to explain the experimental results in the latter systems, one must employ a procedure that combines both relativistic and many-body effects. Such a procedure has been developed and applied[8-10] to a number of transition-metal and rare-earth atoms and ions. The results of these investigations have shown that relativistic effects in general do not give a common enhancement factor[10] for both the valence and the core-electron contributions and that the inter-

play of relativistic and electron-electron interaction effects is more complicated and has to be handled carefully.[8,9]

With the aim to enhance the understanding of hyperfine interactions in alkali-metal atoms, we have investigated rubidium by relativistic many-body perturbation theory. The reason for choosing rubidium for our investigations is that relativistic effects are expected to be important for this relatively heavy system. At the same time, from the trend observed in lithium and sodium,[2] this system will be expected to be subject to substantial contributions from many-body effects. The understanding of rubidium, which is intermediate between potassium and cesium, will also help us obtain conclusions which can be extrapolated and applied to those other two systems. In addition, it is anticipated that a basic quantitative understanding of the various contributions to the hyperfine constant in the ground state of the rubidium atom will be helpful in the analysis of the results for the excited states, which have attracted considerable attention recently.[11-13] Besides the relativistic many-body investigation in rubidium we have also carried out a complete nonrelativistic many-body-perturbation theoretical study. The comparison of the results from both treatments can be expected to give a better understanding of the interplay of relativistic, ECP, and correlation contributions.

The basic aspects of the relativistic many-body perturbation procedure are given in Sec. II and we briefly discuss some of the details pertinent to the application of the procedure to the rubidium atom. The diagrams resulting from the perturbation series are also given in Sec. II and their physical significance is described. The results from the important diagrams are presented in Sec. III. In this section we also discuss the relative importance of the various contributions and the comparison between the results of theory and experiment. Section IV lists the main conclusions of our work.

II. THEORY AND PROCEDURE

A. Relativistic many-body perturbation theory

The principle of the linked-cluster many-body perturbation theory (LCMBPT) and its application to the problem of hyperfine interaction has been described in the earlier literature.[2,14] The emphasis in the past has been mainly on nonrelativistic many-body perturbation theory,[2,15] although recently a number of relativistic calculations have also been reported.[8-10] We will present very briefly here some aspects of our relativistic many-body procedure.

We are interested in the exact solution of the Schrödinger equation

$$\mathcal{H}\Psi = E\Psi , \tag{1}$$

where $\mathcal{H}$ is the net Hamiltonian[16] of the system and can be written as

$$\mathcal{H} = c\sum_i \vec{\alpha}_i \cdot \vec{p}_i + \sum_i \beta_i c^2 - \sum_i \frac{Z}{r_i} + \sum_{i>j} g_{ij} , \tag{2}$$

with

$$g_{ij} = \frac{1}{r_{ij}} - \frac{1}{2r_{ij}}\left(\vec{\alpha}_i \cdot \vec{\alpha}_j + \frac{(\vec{\alpha}_i \cdot \vec{r}_{ij})(\vec{\alpha}_j \cdot \vec{r}_{ij})}{r_{ij}^2}\right). \tag{3}$$

In the subsequent discussion the second term in Eq. (3) (the Breit term) will be dropped in solving the Dirac-Hartree-Fock equation, because the influence was found to be small.[8] The basic principle of the many-body perturbation theory is to write the net Hamiltonian $\mathcal{H}$ as

$$\mathcal{H} = \mathcal{H}_0 + \mathcal{H}' , \tag{4}$$

where $\mathcal{H}_0$ is some chosen one-electron Hamiltonian and $\mathcal{H}'$ is the difference of $\mathcal{H}$ and $\mathcal{H}_0$ to be treated as a perturbation. If Φ_0 is the eigenfunction of the one-electron Hamiltonian $\mathcal{H}_0$ with eigenvalue E_0, we can write

$$\mathcal{H}_0\Phi_0 = E_0\Phi_0 . \tag{5}$$

The solution Ψ of Eq. (1) can be obtained by using the linked-cluster expansion,[14]

$$|\Psi\rangle = \sum_{n=0}^{\infty(L)} \left(\frac{\mathcal{H}'}{E_0 - \mathcal{H}_0}\right)^n |\Phi_0\rangle . \tag{6}$$

With Ψ constructed in this way, the expectation value of an operator $\mathcal{H}_N$ can be written as[2]

$$\langle \mathcal{H}_N \rangle = \sum_{m,n} \langle \Phi_0 | \left(\frac{\mathcal{H}'}{E_0 - \mathcal{H}_0}\right)^m \mathcal{H}_N \left(\frac{\mathcal{H}'}{E_0 - \mathcal{H}_0}\right)^n | \Phi_0 \rangle_L . \tag{7}$$

In order to apply this procedure to obtain a physically measurable quantity represented by the operator $\mathcal{H}_N$, one has to suitably construct $\mathcal{H}_0$, solve for Φ_0 and E_0, and then evaluate the various terms in expression (7). The one-electron Hamiltonian $\mathcal{H}_0$ can be expressed as

$$\mathcal{H}_0 = \sum_{i=1}^{N} T_i + \sum_{i=1}^{N} V_i . \tag{8}$$

In relativistic theory T_i is given by[8]

$$T_i = c\vec{\alpha}_i \cdot \vec{p}_i + \beta_i c^2 - Z/r_i , \tag{9}$$

where Z is the nuclear charge and $\vec{\alpha}$ and β are the usual Dirac spinors. The counterpart of T_i in nonrelativistic theory is

$$T_i = -\tfrac{1}{2}\nabla_i^2 - Z/r_i \,. \tag{10}$$

The V_i chosen in either the relativistic or nonrelativistic case is the standard V^{N-1} potential,[2,15] and the matrix elements of it between states a and b, for example, can be written in the form

$$\langle a|V^{N-1}|b\rangle = \sum_{n=1}^{N-1}\left(\langle an|\frac{1}{r_{12}}|bn\rangle - \langle an|\frac{1}{r_{12}}|nb\rangle\right). \tag{11}$$

However, the one-electron states in nonrelativistic theory are the two-component $|l,m\rangle$ states, while in the relativistic theory they are the Dirac four-component $|jm\rangle$ states. The one-electron basis states are obtained by solving the equation

$$(T+V)\phi_i = \epsilon_i\phi_i \,. \tag{12}$$

The radial relativistic Hartee-Fock equations arising from Eq. (12) are[17]

$$\frac{dP}{dr} + \kappa\frac{P}{r} - \left[c + \frac{1}{c}\left(\frac{Y}{r}+E\right)\right]Q + W_Q = 0 \,, \tag{13}$$

$$\frac{dQ}{dr} - \kappa\frac{Q}{r} - \left[c - \frac{1}{c}\left(\frac{Y}{r}+E\right)\right]P - W_P = 0 \,, \tag{14}$$

where P and Q are, respectively, the large and small components of the wave function. The potential Y and the exchange terms W_P and W_Q are given by[17]

$$Y = Z - \sum_{j'=1}^{N-1}(2j'+1)r\left\langle P_{j'}\left|\frac{1}{r_>}\right|P_{j'}\right\rangle + \left\langle Q_{j'}\left|\frac{1}{r_>}\right|Q_{j'}\right\rangle \tag{15}$$

and

$$W_{P_j \text{ or } Q_j} = -\frac{1}{c}\sum_n\sum_{j'}(2j'+1)(\Gamma j_n j')\left(\left\langle P_{j'}\left|\frac{r_<^n}{r_>^{n+1}}\right|P_j\right\rangle + \left\langle Q_{j'}\left|\frac{r_<^n}{r_>^{n+1}}\right|Q_j\right\rangle\right)\cdot P_{j'} \text{ or } Q_{j'} \,. \tag{16}$$

with

$$\Gamma_{jnj'} = \begin{pmatrix} j & n & j' \\ \frac{1}{2} & 0 & -\frac{1}{2}\end{pmatrix}^2$$

and $r_<$ and $r_>$ standing for the smaller and larger r in the $1/r_{12}$ expansion respectively. The perturbation Hamiltonian $\mathcal{H}'$ is given by

$$\mathcal{H}' = \sum_{i>j}\frac{1}{r_{ij}} - \sum_i V_i \,. \tag{17}$$

The determinant Φ_0 is constructed using the one-electron ϕ_i's corresponding to the lowest energy states. The relativistic ϕ_i's are all $|jm\rangle$ states.[18]

The magnetic hyperfine Hamiltonian is given by[16]

$$\mathcal{H}_N^{\text{rel}} = \sum_i \vec{\alpha}_i \cdot \frac{\vec{\mu}_i \times \vec{r}_i}{r_i^3} \,. \tag{18}$$

The corresponding nonrelativistic expression for alkali-metal atoms with filled core shells and a single s valence electron is given by

$$\mathcal{H}_N^{\text{nr}} = \frac{8\pi}{3}\mu_B\vec{\mu}_i \cdot \sum_i 2\vec{s}_i\delta(r_i) \,. \tag{19}$$

In Eq. (19) note the presence of only the contact term, the orbital and dipolar terms vanishing owing to the spherical symmetry. The experimental measurements[19,20] determine the hyperfine structure utilizing the spin Hamiltonian

$$\mathcal{H}_N = A_J\vec{I}\cdot\vec{J} \,. \tag{20}$$

From Eq. (20) one can write down the following formal expression for the hyperfine constant A_J

$$A_J = (1/IJ)\langle\Psi_J|\mathcal{H}_N|\Psi_J\rangle \,, \tag{21}$$

with $\Psi_J(m_J = J)$, the many-electron wave function in Eq. (6) and with $m_I = I$ for the nucleus. Upon substituting the expansion for Ψ given in Eq. (6) into Eq. (21), one gets a similar expression as in Eq. (7) with $\mathcal{H}_N$ given by Eq. (18) or (19) in the relativistic or nonrelativistic cases, respectively. The summations over m and n generate the various-order diagrams, the physical meanings of which will be discussed in Sec. II B, where their process of evaluation is also described.

B. Diagrammatic procedure

In Sec. II B we shall present briefly the procedure for obtaining the basis set and describe the pertinent diagrams for the rubidium atom and their physical significance. Since the details of obtaining the basis set in the nonrelativistic case is given elsewhere,[2] we shall present only a few important points here. Thus for the choice of the V^{N-1} potential in the present work, it is convenient to create all the angular momentum (l) states in a potential with the $5s$ electron missing. The nonrelativistic basis set consists of bound states

with principal quantum number n up to 12 and twelve continuum states corresponding to a twelve-point Gauss-Laguerre quadrature. The relativistic jm basis set consists of the corresponding $j=l+\frac{1}{2}$ and $j=l-\frac{1}{2}$ functions belonging to the same values of n. For the nonrelativistic as well as the relativistic set, l was chosen to range from 0 to 4. After obtaining the basis set, one evaluates the operator expectation value given in Eq. (7). This is a perturbation expression and, as usual,[2,9] we denote the order of perturbation by the sum $(m+n)$ in Eq. (7), which is also the total number of $1/r_{12}$ interaction lines occurring in the generated diagrams. When $(m+n)$ is equal to zero, the corresponding diagram is shown in Fig. 1 and is referred to as the (0,0) diagram.[2,9] This diagram represents the direct valence-electron contribution to the hyperfine-constant term A_J. From Eq. (21) we find

$$A_J^{\rm rel}(0,0)=-\frac{K_J}{\pi\alpha}\int_0^\infty \frac{P_{5s}Q_{5s}}{r^2}\,dr\,, \tag{22}$$

where α is the fine-structure constant; in order to obtain A_J in units of MHz, K_J can be written as

$$K_J=\frac{8\pi}{3}(\mu_B\mu_I/IJa_B^3h)\times10^{-6}\,, \tag{23}$$

and for the nonrelativistic case,

$$A_J^{\rm nr}(0,0)=K_J\phi_{5s}^2(0)\,. \tag{24}$$

The next-order diagrams result from taking $(m+n)$ equal to 1 in Eq. (7), so either m or n can be equal to one, the other being zero. In effect we need to consider only one of these possibilities to draw the diagrams shown in Fig. 2 and then multiply the values of these diagrams by 2. The digram shown in Fig. 2(a) is referred to as a phase-space[2] diagram because the excitation to $5s^-$ is possible owing to the occupation of the $5s^+$ in the shell with the same principal quantum number. The diagram in Fig. 2(b) represents the ECP effect which arises owing to the exchange interaction of the unpaired $5s$ valence electron with other core s states. Both of these diagrams exist in the relativistic and nonrelativistic formalisms. For example, the expression for the diagram in Fig. 2(b) is

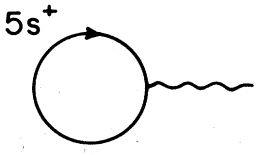

FIG. 1. (0,0) diagram.

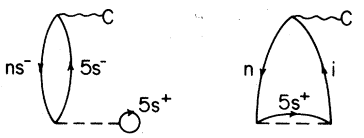

FIG. 2. Core polarization or (0,1) diagrams.

$$A_J(0,1)=2K_J\sum_i\frac{\rho_{ni}I_{ni}}{\epsilon_n-\epsilon_i} \tag{25}$$

for the nth core state. The entities ρ and I are defined[2,9,17] by the following equations, in which nr stands for the nonrelativistic, rel for the relativistic formulation:

$$\rho_{ni}^{\rm rel}=-\frac{1}{2\pi\alpha}\left(\int_0^\infty\frac{P_nQ_i}{r^2}\,dr+\int_0^\infty\frac{P_iQ_n}{r^2}\,dr\right), \tag{26}$$

$$\rho_{ni}^{\rm nr}=\langle\phi_n|\,\delta(r)\,|\phi_i\rangle\,, \tag{27}$$

$$I_{ni}^{\rm rel}=\langle(P_{ns}P_{5s}+Q_{ns}Q_{5s})\,|\,1/r_{12}\,|\,(P_{5s}P_i+Q_{5s}Q_i)\rangle\,, \tag{28}$$

$$I_{ni}^{\rm nr}=\langle\phi_n\phi_{5s}|\,1/r_{12}\,|\,\phi_{5s}\phi_i\rangle\,. \tag{29}$$

In the relativistic formulation there are also contributions to the ECP from other than s shells due to Casimir-type distortions of the atom.[8] In the present case only the contributions from the p shells are important. For the sake of completeness we list here the expression[21] for $\rho_{ni}^{\rm rel}$ when the hole state n is not an s state.

$$\rho_{ni}^{\rm rel}=\frac{3}{4\pi\alpha}\left(\int_0^\infty\frac{P_nQ_i}{r^2}\,dr+\int_0^\infty\frac{P_iQ_n}{r^2}\,dr\right)\left(\frac{4l_i}{4l_i^2-1}\right)(m_j)_i\,, \tag{30}$$

for $l_i=j_i+\frac{1}{2}$ and

$$\rho_{ni}^{\rm rel}=-\frac{3}{4\pi\alpha}\left(\int_0^\infty\frac{P_nQ_i}{r^2}\,dr+\int_0^\infty\frac{P_iQ_n}{r^2}\,dr\right)\times\left(\frac{4(l_i+1)}{(2l_i+1)(2l_i+3)}\right)(m_j)_i\,, \tag{31}$$

for $l_i=j_i-\frac{1}{2}$

We now proceed to the description of second-order diagrams where two orders of $1/r_{12}$ interaction lines will occur and which correspond to $(m+n)$ equal to 2 in the perturbation-series expression (7). These diagrams are shown in Figs. 3 and 4. In obtaining the second-order diagrams one can either have m or n equal to two, the other being zero, or have $m=n=1$. The diagrams of

the former type are shown in Fig. 3 and are known as (0, 2) diagrams, whereas the latter type, known as (1, 1) diagrams, are shown in Fig. 4. In either type there are two distinct categories, one representing a purely one-electron-type excitation, the other representing correlation-type excitations. The one-electron diagrams are shown in Figs. 3(a)–3(h) and 4(a)–4(d). Of these one-electron diagrams, some are considered as corrections to the (0, 1) diagrams and are known[2] as laddering diagrams. In general they represent potential corrections to hole and particle states used in evaluating the (0, 1) diagrams, for instance 3(b) and 3(c). Diagrams 3(a), 3(d), and 3(e) with hole states m and n from the same shell (but different spin) represent potential corrections and are included in laddering; otherwise these diagrams, as well as those shown in 3(f)–3(h), 4(a), and 4(b), are known as consistency diagrams[2,21] because the polarized shell n in turn produces a polarization of shell m. In diagrams of type 4(a), 3(f), and 3(g), either the hole state m should be a $5s^+$ state or the particle state i a $5s^-$ state except, of course, in some special cases where, for example, the state m can be a $4s^-$ and n a $4s^+$ state. Diagrams 4(c) and 4(d) represent second-order ECP effects.

Diagrams 3(i)–3(l) and 4(e)–4(j) represent correlation effects.[2] In each of these diagrams there are always two simultaneously excited states and this represents dynamic correlation between those states. As will be seen from the results in Sec. III, the role of these diagrams in the case of rubidium is very crucial in order to explain the observed hyperfine constant in this system. In diagrams 3(i) and 3(k) either the state shown as m must be the $5s^+$ state or the state i must be a $5s^-$, while in diagrams 3(j), 3(l), 4(e), and 4(f), m or n can be $5s^+$ or i should be a $5s^-$ particle state.

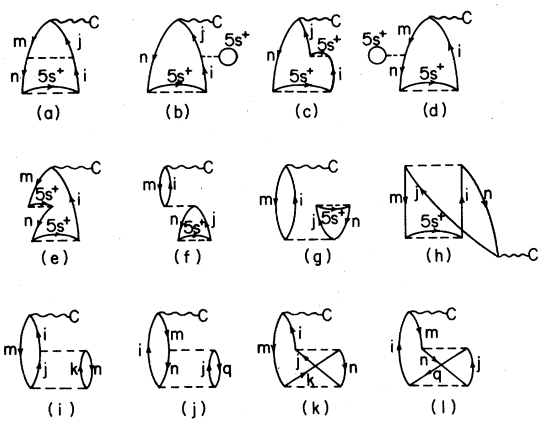

FIG. 3. Typical (1,1) diagrams.

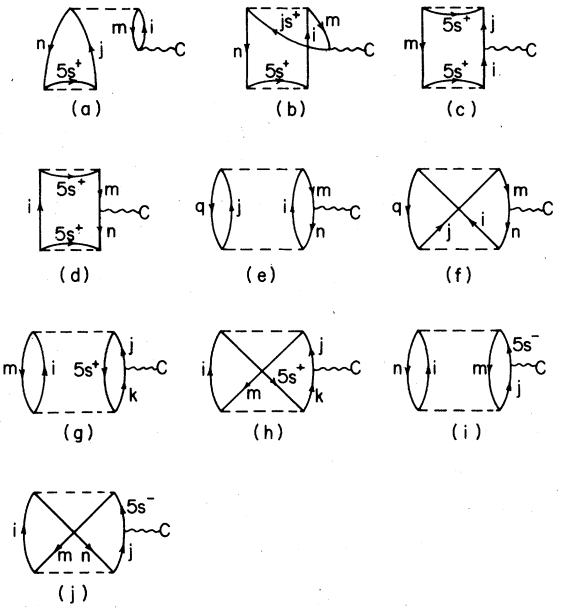

FIG. 4. Typical (0,2) diagrams.

There are more diagrams [3(g) and 3(h)] that look like, but do not represent correlation effects, and this can be revealed by unfolding them.[2] It can also be observed that in all the hyperfine diagrams in Figs. 1–4, as well as the higher-order ones in Fig. 5, at least one $5s$ hole state or one $5s$ particle state has to take part, since the $5s$ electron is the one which produces the net spin density in the system. For purposes of economy in computing time, in evaluating the diagrams relativistically we have assumed that the $j = l - \frac{1}{2}$ orbitals have the same radial characters as $j = l + \frac{1}{2}$ orbitals. Earlier work[8-10] has shown that the error made by this approximation is less than 2%.

The contributions from all the diagrams up to second order that have just been discussed, in-

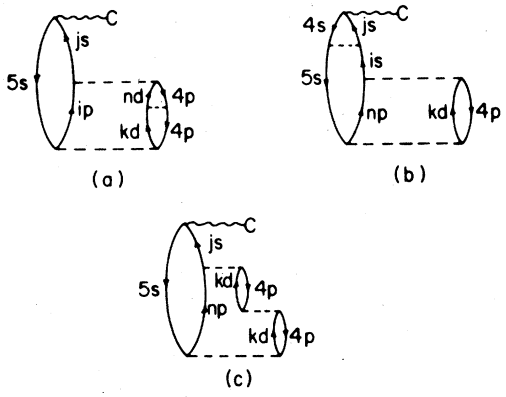

FIG. 5. Higher-order diagrams.

cluding potential-correction laddering effects, are described in Sec. III. In addition, we have also studied third- and higher-order diagrams such as, for example, those shown in Fig. 5, whose importance is also discussed in Sec. III.

III. RESULTS AND DISCUSSION

In Secs. I and II, we have discussed the theory and procedure for evaluating the hyperfine diagrams relativistically and nonrelativistically, and we now proceed to present the results. We will start with the zero-order and subsequently proceed to the ECP, consistency, correlation, and higher-order contributions. In each stage we would like to present the nonrelativistic results, the relativistic modification as represented by the difference between the corresponding relativistic and nonrelativistic results, and try to analyze all the results in terms of physical effects. In doing so we shall try to draw specific conclusions about the importance of one-particle, many-body, and relativistic effects for the hyperfine interaction in rubidium. Combining our conclusions with those of earlier investigations on lighter alkali-metal atoms,[2,4] we will then extrapolate our ideas to make general statements about the nature of hyperfine interactions in alkali-metal systems.

In evaluating the results of the contact hyperfine-interaction constant A_J in both relativistic and nonrelativistic theory, one needs the value of the multiplying factor K_J defined in Eq. (23). Using the values of the currently available constants,[23] K_J was found to be 1467.630 MHz/a.u. After evaluating each diagram in atomic units, we multiply its value by this constant.

In the rubidium atom, there is an unpaired $5s$ valence electron which alone makes a large contribution to the hyperfine constant in the restricted Hartree-Fock theory. In the LCMBPT language, this is the (0, 0) diagram which is shown in Fig. 1. The contribution to this diagram was found to be

$$A_J^{\mathrm{rel}}(0,0) = 2\ 255.41 \text{ MHz}$$

and

$$A_J^{\mathrm{nr}}(0,0) = 1\ 880.63 \text{ MHz}$$

from relativistic and nonrelativistic calculations, respectively. There is thus an enhancement of 20% of the result due to relativistic effects, in reasonable agreement with earlier estimates in the literature.[5,6] This enhancement represents only the influence of the contraction of the radial function associated with the $5s$ orbital, in the Hartree-Fock approximation, due to relativistic effects. For understanding the net relativistic effect, one has to evaluate relativistically the higher-order diagrams in Figs. 2–5 involving various orders of electron-electron interaction.

We have listed the ECP results that arise due to the polarization of $1s$–$4s$ cores by the exchange interaction with $5s$ in Table I. In this table we give the results for both relativistic and nonrelativistic diagrams, each being further classified into laddered and unladdered categories. We have briefly explained in Sec. II B the procedure for laddering, and the laddered values listed in this table are obtained by a geometric-series approximation for a converging infinite series of diagrams. In the case of s states each row includes the contribution from both the usual ECP represented by Fig. 2(b) and the phase-space diagram[22] shown in Fig. 2(a). The net relativistic ECP contribution arising from p-core states is also presented in Table I; this does not have a corresponding counterpart in the nonrelativistic case because the p-orbital wave functions vanish at the origin in the nonrelativistic approximation. In the last column of Table I we have presented the ratio of relativistic to nonrelativistic results for the ECP diagrams. It is interesting to note that for the case of $1s$ and $2s$ states there is a deenhancement instead of the enhancement factor that is observed for $\phi_{5s}^2(0)$. In the case of the $3s$ and $4s$ states, however, there are enhancements of 19%

TABLE I. Contribution (in MHz) of the exchange-core-polarization to the hyperfine constant of ^{87}Rb.

States	$a_{\mathrm{ECP}}^{\mathrm{nr}}$ unladdered	$a_{\mathrm{ECP}}^{\mathrm{rel}}$ unladdered	$a_{\mathrm{ECP}}^{\mathrm{nr}}$ laddered	$a_{\mathrm{ECP}}^{\mathrm{rel}}$ laddered	$\frac{a_{\mathrm{ECP}}^{\mathrm{rel}}}{a_{\mathrm{ECP}}^{\mathrm{nr}}}$
$1s$	6.9	5.2	7.0	5.2	0.74
$2s$	29.6	28.8	29.6	28.9	0.98
$3s$	68.9	81.7	73.8	87.8	1.19
$4s$	217.8	270.7	261.1	320.9	1.23
np	...	2.6	...	2.6	...
Total	323.2	389.0	371.5	440.2	1.19

and 23% respectively, which are close to the enhancement factor of 20% for the contact $5s$ case mentioned in the previous paragraph. These different trends for the ECP contributions from $1s$ and $2s$ states on the one hand and $3s$ and $4s$ on the other are worth further examination. Thus a decrease, of a type similar to the ECP results for $1s$ and $2s$ state was also observed earlier in the case of the manganese atom.[9] However, in strong contrast to the cases[8-10] of Mn^0, Eu^0, and Gd^{3+} where all s shells have very different enhancement factors, we find for $3s$, $4s$, and $5s$ (direct contribution) shells approximately the same factor. Further understanding of the relativistic effects in the ECP diagrams can be achieved by looking at the individual integrals involved in these diagrams. The ECP effect is the product of three factors, namely, the integral representing the hyperfine vertex (ρ), the exchange integral (I), and the inverse of the energy differences. In Tables II and III we have presented these quantities for a chosen set of $ns \rightarrow is$ excitations obtained both relativistically and nonrelativistically. Table II lists the factors ρ and I defined by Eqs. (26)–(29). In the fifth column we have presented the ratios of the relativistic to nonrelativistic hyperfine vertex integrals and in the last column similar ratios for exchange integrals are presented. The ratios of the ρ's are nearly constant around the value of 1.19, as is expected,[5,6] and a constant ratio was also found in the Mn^0, Eu^0, and Gd^{3+} cases.[8-10] However, the behavior of the exchange integral is rather different. For $3s$ and $4s$ states, we hardly find any relativistic effect. In contrast to the cases Mn^0, Eu^0, and Gd^{3+} studied earlier,[8,9] in the alkali-metal atom Rb the polarized shells and polarizing shell have the same l value and, presumably, the same relativistic contraction (particularly the $3s$, $4s$, and $5s$ shells), and hence the overlap between the $5s$ and the core $4s$ and $3s$ shells, important for exchange interaction, does not change very much in going to relativistic theory. The deenhancements observed for the $1s$ and $2s$ ECP contributions also become understandable from the results in Table II, since the exchange integrals I involved in the case of $1s$ and $2s$ shells undergo substantial decreases in going to relativistic theory. A similar trend was also observed in the cases of transition-metal and rare-earth atoms.[8,9] We shall remark next on the influence of the third factor, namely, the change in the energy denominators $\Delta\epsilon$ on the ECP results. It is seen from the last column of Table III that the relativistic effect changes the values of $\Delta\epsilon$ very little.

The net result from the (0, 1) diagram is 371.5 MHz nonrelativistically and 440.2 MHz relativistically. The nonrelativistic ECP result can be compared with the results obtained recently[24] by a moment-perturbation (MP) method, namely, 437.85 MHz. This result is in reasonable agreement with our nonrelativistic 371.51 MHz. The difference of about 18%, as discussed earlier,[8] is most likely a consequence of the local Sternheimer approximation used in the MP procedure. Earlier nonrelativistic calculations have shown that the ratio $A_{\mathrm{ECP}}/A_{\mathrm{direct}}$ was nearly constant in the series sodium to cesium. Our observation in the present work that relativistic effects do not change $A_{\mathrm{ECP}}/A_{\mathrm{direct}}$ significantly indicates that the relativistic value of this ratio should also be reasonably constant in the series sodium to cesium.

Combining the contributions from the direct

TABLE II. Comparison of a sample of relativistic and nonrelativistic hyperfine-vertex integrals ρ and exchange integrals I defined in Eqs. (26)–(29).

ns	is	ρ^{nr}(a.u.)	ρ^{rel}(a.u.)	Ratio	I^{nr} (10^{-5} a.u.)	I^{rel} (10^{-5} a.u.)	Ratio
1	5	141.80	164.10	1.15	0.598	0.368	0.61
	6	73.40	84.36	1.14	0.269	0.238	0.88
	7	47.03	53.94	1.14	0.170	0.154	0.91
2	5	44.73	53.04	1.19	2.107	1.507	0.72
	6	23.15	27.27	1.18	1.104	1.023	0.93
	7	14.84	17.43	1.17	0.707	0.668	0.94
3	5	18.11	21.52	1.19	12.468	9.929	0.80
	6	9.38	11.06	1.18	6.437	6.145	0.95
	7	6.01	7.07	1.18	4.118	3.99	0.97
4	5	6.12	7.28	1.18	157.567	166.8	1.06
	6	3.17	3.74	1.18	80.287	82.9	1.04
	7	2.03	2.39	1.18	51.119	52.8	1.03

TABLE III. Comparison between nonrelativistic and relativistic one-electron energy differences (a.u.).

States	$\Delta\epsilon_{nr}$	$\Delta\epsilon_{rel}$	Ratio
$1s-6s$	−551.63	−562.31	1.019
$2s-6s$	−75.21	−77.66	1.032
$3s-6s$	−12.29	−12.72	1.035
$4s-6s$	−1.67	−1.71	1.024

(0, 0) and the ECP (0, 1) diagrams, we obtain a net result of 2252.14 MHz from our nonrelativistic calculation and 2695.6 MHz from the relativistic work. Comparing this relativistic result with the experimental result of 3417.3 MHz, we find that the difference is larger than the ECP contribution and one, therefore, expects very significant contributions from second- and higher-order diagrams.

The second-order results of our calculation are listed in Tables IV and V. We consider first the results from the consistency diagrams shown in Figs. 3 and 4 which we have listed in Table IV. We have quoted only the contributions from the diagrams which contribute individually more than 1 MHz in magnitude. The rest of the diagrams are summed and their net contribution labeled "other diagrams", and listed in this table. As shown in Table IV, the total result from the (0, 2) consistency diagrams is 9.20 MHz and from the (1, 1) consistency diagrams is 3.23 MHz, adding up to the net result of 12.43 MHz from all second-order consistency diagrams. This result is only about 3% of the (0, 1) nonrelativistic contribution. Owing to the smallness of this result, we felt it not necessary to evaluate these diagrams relativistically. A reasonably good estimation of the relativistic enhancement effect for these diagrams can be made by applying a multiplication factor of 1.19 (as in the ECP case) to the nonrelativistic result of 12.43 MHz. Thus we obtain a relativistic result of 14.3 MHz. This result shows that the consistency effect is small, and the net one-electron results, combining all the contributions discussed so far, are 2264.56 MHz from the nonrelativistic diagrams and 2709.94 MHz from the relativistic diagrams.

TABLE IV. Contributions (in MHz) to the hyperfine constant of ^{87}Rb second-order consistency diagrams. The results presented in this table are from nonrelativistic calculations. Only diagrams of magnitude larger than 1 MHz are individually listed.

Diagram	States	Contribution
3(a)	$m=5s^+n=4s^+$	1.26
	$m=5s^+n=4p^+$	5.81
	$m=4s^+n=4p^+$	−9.97
	$m=3s^+n=4s^+$	3.97
3(f)	$m=4s^-n=4s^+$	−1.67
	$m=5s^+n=4p^+$	8.78
3(g)	$m=4s^-n=4s^+$	2.45
	$m=4s^-n=4p^+$	−1.52
Other (0, 2) consistency		0.10
Total (0, 2) consistency		9.20
4(a)	$m=5s^+n=4p^+$	1.73
	$m=4s^-n=4s^+$	2.94
	$m=4s^-n=4p^+$	−1.81
Other (1, 1) consistency		0.38
Total (1, 1) consistency		3.23
Net total consistency		12.42

The diagrams shown in Figs. 3(i)–3(l) and 4(e)–4(j) represent dynamic correlation effects. From an inspection of the results so far one can expect a sizeable contribution from these correlation diagrams. Due to the large number of diagrams present in this class, a complete relativistic evaluation is very cumbersome. We have evaluated all of them with the nonrelativistic basis set. However, we have evaluated some major contributing correlation diagrams with the relativistic basis set and compared the results with those from the nonrelativistic calculation to examine if we could still use a common enhancement factor in order to incorporate the relativistic effect. This procedure was based on the trend observed in the evaluation of the (0, 0) and (0, 1) diagrams. The major contributing diagrams involve the $n=4$ and $n=5$ shells, and our results in the (0, 0) and (0, 1) diagrams show that, particularly for these shells, a relativistic enhancement factor is applicable.

In Table V we have presented the nonrelativistic results of the correlation diagrams. The diagrams that contribute more than 10 MHz in magnitude are listed individually[25] and the rest are included in the list as "other diagrams." The major contributing diagrams are those which involve the $5s$-hole state at the hyperfine vertex correlating with the $4s$, $4p$, or $3d$ shells. This result can be understood from two main considerations. The first is that the $5s$ state is unpaired and thus has a net density at the nucleus, and also, being the most deformable state, is subject to large correlation. Secondly, the $4s$, $4p$, and $3d$ states are closest to $5s$ and, therefore, correlation diagrams involving these states are the major ones. Thus it can be observed from Table V that through correlation, a $4p$ state alone can modify the Hartree-Fock $5s$ result (0, 0) by as much as 36%. The total results from the (0, 2) and (1, 1) nonrelativistic correlation diagrams are 610.4 and 5.8 MHz respectively, leading to a net result of 616.2 MHz. As pointed out earlier, we have examined the relativistic modification of the correlation effect by making relativistic evaluations of the diagrams which

TABLE V. Contributions from second-order correlation diagrams to the ^{87}Rb hyperfine constant. The results listed are from nonrelativistic calculations. Only the diagrams of magnitude larger than 10 MHz are listed (Ref. 25).

Diagram	States			Contribution
3(i)	$m=5s^+$	$n=4s^+$		81.3
		$n=4p$		672.3
		$n=3d$		165.0
	$m=4s^-$	$n=4s$	$i=5s^-$	−12.8
		$n=4p$	$i=5s^-$	−90.0
		$n=3d$	$i=5s^-$	−38.6
3(j)	$m=5s^+$	$n=4s^+$		−60.6
		$n=4p^+$		−39.2
	$m=4s^+$	$n=5s^+$		−27.6
	$m=4s^-$	$n=4s^-$	$i=5s^-$	51.8
		$n=4p^-$	$i=5s^-$	17.1
Other (0,2) direct correlation				−8.7
Total (0,2) direct correlation				710.0
3(k)	$m=5s^+$	$n=4p$		−60.2
		$n=4s$		−25.3
		$n=3d$		−14.7
	$m=4s^+$	$n=5s^+$		−19.4
	$m=4s^-$	$n=4p^-$	$i=5s^-$	17.4
3(l)	$m=5s^+$	$n=4p^+$		11.2
	$m=4s^-$	$n=4p^-$	$i=5s^-$	−12.7
Other (0,2) exchange correlation				4.1
Total (0,2) exchange correlation				−99.6
4(e)	$m=5s^+$	$n=5s^+$		−17.0
		$n=4s^+$		−17.1
4(g)	$m=4p$			31.2
4(i)	$m=4s$			−11.6
Other (1,1) correlation				20.3
Total (1,1) correlation				5.8
Net total second-order correlation				616.2

make the major contribution in the nonrelativistic case. The relativistic enhancement factors for all these diagrams are found to be positive and lie around 15%. We, therefore, have applied a relativistic enhancement factor of 15% to the nonrelativistic values of the rest of the correlation diagrams to account for their relativistic modification. Following this procedure, the net relativistic correlation contribution up to the second order is found to be 708.5 MHz. Including this, the net result up to second order (including laddering effects for the ECP diagrams) is 3418.4 MHz. The net contributions from various physical effects to the hyperfine constant are presented in Table VI.

To obtain an estimate of higher-order effects, we have evaluated a number of diagrams (Fig. 5(a) which can be considered as potential-ladder corrections to some of the correlation diagrams, as well as some additional higher-order diagrams [such as Figs. 5(b) and 5(c)]. The net contribution from these types of diagrams is found to be about 40 MHz. Since there can be a large number of such diagrams and we expect them to be individually smaller than the ones we have considered, we have used a conservative error limit of 25 MHz to incorporate their effect. Combining this with the possible influence of computational limitations such as, for example, a finite number of basis-set functions, we have ascribed a confidence limit of ±50 MHz to our theoretical result of 3458.4 MHz for the hyperfine constant.

TABLE VI. Summary of results for the hyperfine constant of ^{87}Rb (in MHz).

Diagrams	nr	rel	$\frac{\text{rel}-\text{nr}}{\text{rel}}$
(0,0)	1880.6	2255.4	0.20
(0,1) laddered	371.5	440.2	0.20
Consistency	12.4	14.3	0.15
Correlation	616.2	708.5	0.15
Higher order	35.0	40	0.14
Net total	2915.7	3458.4	0.19
Experiment		3417.3	

IV. CONCLUSIONS

In summary, the net result for the hyperfine constant of the rubidium (^{87}Rb) atom from the present calculation is 3460 ±50 MHz. This result is in good agreement with the experimental value 3417.3 MHz.[20] There are four mechanisms that have been found to give important contributions: the direct effect (A_d) coming from the valence electron, the ECP effect (A_{ECP}) from the polarization of the core electrons, correlation effects (A_{corr}), especially between the valence electron and the outer p shell, and relativistic modifications of these effects.

Several trends have been observed from our analysis. In comparison with earlier work,[2,4] we conclude that for the alkali-metal atoms, the ratio A_{ECP}/A_d is nearly constant in the nonrelativistic and relativistic formulation, with the exception of lithium. We further observe that the correlation contribution A_{corr} increases relative to A_d in going to heavier systems. From the observed trend in this respect up to rubidium, it is expected that the contribution from correlation effects in cesium would be significantly larger relative to the direct contribution than the 30% found in rubidium and perhaps as large as 40% in the heaviest alkali-metal francium. A third important fact is the very small variation in the relativistic enhancement factor for ECP contributions from different s-core shells of rubidium. This is in marked contrast to the corresponding results found earlier in the transition-metal series.[10] This difference in behavior between rubidium and the transition metals is due to the s character of the polarizing shell in the former, a consequence of this being that the polarizing and polarized shells have comparable relativistic contractions.

Finally, in view of the importance of correlation effects and the relativistic modifications of ECP and correlation effects observed in the present work on the rubidium atom, one can expect that these effects will be significant in rudibium metal in particular and alkali metals in general, and would have to be considered in attempting to explain the remaining differences[3] between the theoretical and experimental Knight shift and relaxation-time data in these metals.

ACKNOWLEDGMENT

This work was supported by the National Science Foundation.

---

*Present address: Computer Sciences Corp., Silver Spring, Md. 20910.

[1]*Hyperfine Interactions*, edited by A. J. Freeman and R. B. Frankel (Academic, New York, 1967).

[2]E. S. Chang, R. T. Pu, and T. P. Das, Phys. Rev. 174, 1 (1968); T. Lee, N. C. Dutta, and T. P. Das, Phys. Rev. A 4, 995 (1970).

[3]S. D. Mahanti, L. Tterlikkis, and T. P. Das, *Magnetic Resonance*, edited by C. K. Coogan *et al.* (Plenum, New York, 1970); S. D. Mahanti and T. P. Das, Phys. Rev. B 3, 1599 (1971).

[4]L. Tterlikkis, S. D. Mahanti, and T. P. Das, Phys. Rev. 176, 10 (1968).

[5]H. Kopfermann, *Nuclear Moments* (Academic, New York, 1968).

[6]J. P. Desclaux, At. Data 12, 311 (1973).

[7]An extensive list of references of work on hyperfine interactions in lithium is available in E. S. Chang *et al.* Ref. 2.

[8]J. Andriessen, D. van Ormondt, S. N. Ray, and T. P. Das, J. Phys. B 11, 2601 (1978); J. Andriessen, K. Raghunathan, S. N. Ray, and T. P. Das, Phys. Rev. B 15, 2533 (1977).

[9]J. Andriessen, S. N. Ray, T. Lee, T. P. Das, and D. Ikenberry, Phys. Rev. A 13, 1669 (1976).

[10]J. Andriessen, D. van Ormondt, S. N. Ray, K. Raghunathan, and T. P. Das, J. Phys. B 10, 1979 (1977).

[11]K. H. Liao, R. Gupta, and W. Happer, Phys. Rev. A 8, 2792 (1973); R. Gupta, W. Happer, L. K. Ham, and S. Svanberg, *ibid.* 8, 2811 (1973); K. H. Liao, L. R. Lam, R. Gupta, and W. Happer, Phys. Rev. Lett. 32, 1340 (1974).

[12]T. Lee, J. E. Rodgers, T. P. Das, and R. M. Sternheimer, Phys. Rev. A 14, 51 (1976).

[13]I. Lindgren, J. Lindgren, and A. M. Märtensson, Z. Phys. A 279, 113 (1976).

[14]J. Goldstone, Proc. R. Soc. A 239, 267 (1957).

[15]H. P. Kelly, Phys. Rev. 136, B896 (1964).

[16]T. P. Das, *Relativistic Quantum Mechanics of Electrons* (Harper and Row, New York, 1973).

[17]I. P. Grant, Proc. R. Soc. A 262, 555 (1961).

[18]In the present system with a single electron outside closed shells, a single determinantal function Φ_0 is appropriate for the one-electron approximation. For open-shell systems, with more than one electron outside closed shells, in nonrelativistic and particularly in relativistic theory, the multielectron wave function in the one-electron approximation would usually involve more than one determinant. However, for hyperfine properties in nonrelativistic theory, one can often work with single-determinant wave functions by choosing the highest m_J, and the hyperfine constants for different J states are related through Clebsch-Gordan coefficient-dependent factors [J. D. Lyons *et al.*, Phys. Rev. 178, 103 (1968); 186, 266 (1969)]. For relativistic theory the multideterminant nature for open shells is difficult to avoid if one works with jm states. For moderately heavy atoms, however, this problem can be handled by working with the relativistically coupled ls orbitals [J. Andriessen and D. van Ormondt, J. Phys. B 8, 1993 (1975)].

[19]J. Callaway, *Energy Band Theory* (Academic, New York, 1964).

[20]S. Penselin *et al.*, Phys. Rev. 127, 524 (1962); R. Gup-

ta, R. Chang, and W. Happer, Phys. Rev. A 6, 529 (1972); E. Arimondo, M. Inguscio, and P. Violino, Rev. Mod. Phys. 49, 31 (1977).
[21]M. E. Rose, *Relativistic Electron Theory* (Wiley, New York, 1961).
[22]S. N. Ray, T. Lee, and T. P. Das, Phys. Rev. A 7, 1469 (1973).
[23]O. Lutz, Phys. Lett. A 25, 440 (1967); B. N. Taylor, W. H. Park, and D. N. Langenberg, Rev. Mod. Phys. 41, 375 (1969).
[24]C. F. Mulks, T. Lee, and T. P. Das, Phys. Rev. A 13, 1271 (1976).
[25]The limit of 10 MHz is used for listing the correlation diagrams individually as compared to 1 MHz for the consistency diagrams because the former are, in general, an order of magnitude larger than the latter.